

Selective corticostriatal plasticity during acquisition of an auditory discrimination task

Qiaojie Xiong^{1*}, Petr Znamenskiy^{1,2*} & Anthony M. Zador¹

Perceptual decisions are based on the activity of sensory cortical neurons, but how organisms learn to transform this activity into appropriate actions remains unknown. Projections from the auditory cortex to the auditory striatum carry information that drives decisions in an auditory frequency discrimination task¹. To assess the role of these projections in learning, we developed a channelrhodopsin-2-based assay to probe selectively for synaptic plasticity associated with corticostriatal neurons representing different frequencies. Here we report that learning this auditory discrimination preferentially potentiates corticostriatal synapses from neurons representing either high or low frequencies, depending on reward contingencies. We observe frequency-dependent corticostriatal potentiation *in vivo* over the course of training, and *in vitro* in striatal brain slices. Our findings suggest a model in which the corticostriatal synapses made by neurons tuned to different features of the sound are selectively potentiated to enable the learned transformation of sound into action.

Animals use sensory information to guide their behaviour. The neural mechanisms underlying the transformation of sensory responses into motor commands have been studied extensively using a two-alternative forced-choice task, in which subjects are trained to make a binary decision and indicate their choice by performing one of two actions. Defined brain areas have been implicated in the circuit performing this transformation in primates^{2,3} and rodents^{1,4–10}.

Striatal plasticity has been implicated in reinforcement learning^{11,12}, specifically at corticostriatal inputs^{13,14}, but the site or sites of plasticity engaged when animals learn to make appropriate decisions about sensory stimuli are not well established. We previously found that neurons in the primary auditory cortex projecting to the auditory striatum drive decisions in a two-alternative forced-choice auditory task¹ in which rats learn to associate the frequency of a complex auditory stimulus with either a left or right reward port (Fig. 1a, b). We hypothesized that plasticity of auditory corticostriatal connections encodes the association between frequency and the rewarded response.

To test this hypothesis, we developed a novel *in vivo* recording method with which we could monitor the strength of corticostriatal synapses, in a way that did not depend on the activity of cortical neurons. We used this to measure synaptic strength in single animals over multiple behavioural sessions during the course of learning. We first injected an adeno-associated virus expressing channelrhodopsin-2 (AAV-ChR2-Venus) into the left primary auditory cortex. This resulted in widespread expression of ChR2 in different cell types in the auditory cortex, including corticostriatal neurons and their axons in the striatum (Extended Data Fig. 1). We next implanted bundles of optical fibres and tetrodes into the left auditory striatum (Fig. 1c). Brief pulses of blue light delivered through the optical fibre excited the corticostriatal axons and elicited excitatory postsynaptic responses in the striatum (Fig. 1d). Because the striatum, like the CA1 region of the hippocampus, lacks recurrent excitatory connections, we reasoned that this *in vivo* ChR2-evoked local field potential response (ChR2-LFP) could serve as a measure of the strength of the corticostriatal synaptic connectivity¹⁵. The ChR2-LFP

had a stereotypic waveform consisting of an early and a late component (Extended Data Fig. 2a). Local pharmacological blockade of excitatory but not inhibitory transmission diminished the late component, indicating that it was mainly mediated by currents elicited by glutamatergic release from corticostriatal terminals (Fig. 1d and Extended Data Fig. 2c). The early component was resistant to all blockers including tetrodotoxin, suggesting that it is driven directly by light-evoked ChR2 currents in corticostriatal axons. The early component was not observed in the absence of ChR2 (Extended Data Fig. 3), indicating that it was not due to a photoelectric artefact, and its amplitude increased with increasing photostimulation (Extended Data Fig. 4). In subsequent analyses we normalized the ChR2-LFP to the amplitude of the early component (Extended Data Fig. 2a) to correct for fluctuations in the number of ChR2-expressing fibres recruited, and then used the initial slope of the second component as a measure of corticostriatal synaptic efficacy (Fig. 1d and Extended Data Fig. 2b). This metric was robust to changes in light intensity and was proportional to the intracellular excitatory postsynaptic current, indicating that it was a good measure of synaptic strength (Extended Data Fig. 4).

We used the ChR2-LFP to assess changes in the strength of corticostriatal synapses over the course of training in the cloud-of-tones task.

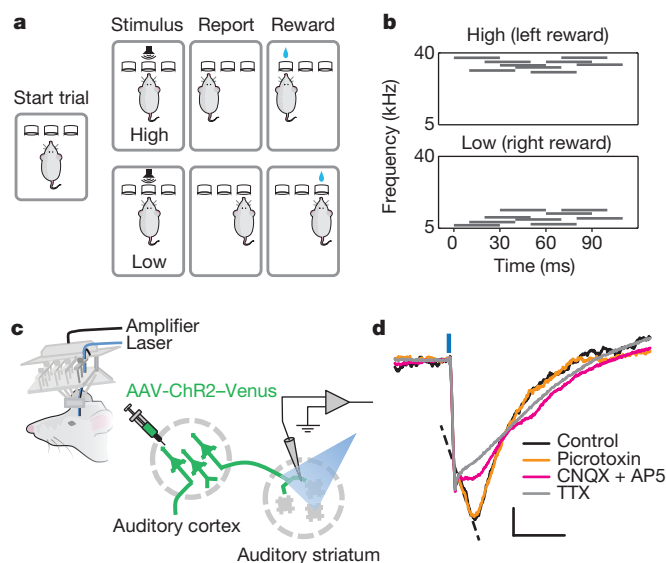


Figure 1 | Dissection of ChR2-LFP *in vivo*. **a**, Cloud-of-tones task. **b**, Example spectrograms of cloud-of-tones stimuli. **c**, Recording method to examine corticostriatal synaptic strength *in vivo*. **d**, ChR2-LFP recorded from auditory striatum under control conditions (black trace) and after application of picrotoxin (orange), CNQX (6-cyano-7-nitroquinoxaline-2,3-dione) and AP5 (2-amino-5-phosphonoverate) (pink), and tetrodotoxin (TTX, light grey). The slope of the CNQX/AP5-sensitive component was used to quantify corticostriatal synaptic strength (dotted line). Scale bars, 20 μV, 5 ms.

¹Cold Spring Harbor Laboratory, 1 Bungtown Road, Cold Spring Harbor, New York 11724, USA. ²Watson School of Biological Sciences, Cold Spring Harbor Laboratory, 1 Bungtown Road, Cold Spring Harbor, New York 11724, USA.

*These authors contributed equally to this work.

After establishing a stable baseline over several days in naive rats, we measured the ChR2-LFP after each training session. We used the tone-evoked multiunit responses recorded before training to estimate the frequency tuning at each site (see Methods). At some recording sites, corticostriatal synaptic efficacy increased as soon as the animal started to learn the task, and continued to increase in subsequent training sessions (Fig. 2a). Synaptic efficacy at such sites thus reflected behavioural performance over the course of training. At other sites, however, corticostriatal efficacy remained unchanged over the course of training (Fig. 2b). We found that potentiation was restricted to sites tuned to low-frequency (<14 kHz, the centre frequency used in the task) sounds (mean potentiation 30%; $n = 17$, $P = 0.002$, signed-rank test, Fig. 2c), whereas sites tuned to high-frequency (>14 kHz) sounds showed no significant change (mean change -3%; $n = 6$, $P = 0.58$, signed-rank test, Fig. 2c). Notably, all animals in this cohort were trained to associate low-frequency sounds with rightward choices (LowRight), and all recordings were performed in the left striatum. Hence, low frequencies were always associated with choices contralateral to the recording hemisphere. Our results therefore suggest that task training selectively enhances the strength of corticostriatal synapses only when the stimuli they encode are associated with contralateral choices (Fig. 2d).

The observed potentiation depended strongly on the frequency tuning of the recording site, suggesting that corticostriatal plasticity encodes the association of specific frequencies with rewarded actions. However, since the striatum has been widely implicated in motor learning¹⁴, we sought to rule out this and other alternative causes of plasticity unrelated to auditory discrimination. We trained animals to perform a simple two-alternative forced-choice visual task, relying on the same sequence of movements, and monitored the strength of auditory corticostriatal synapses during learning (Fig. 3a). There was no significant change in ChR2-LFP in the auditory striatum during visual task training (mean

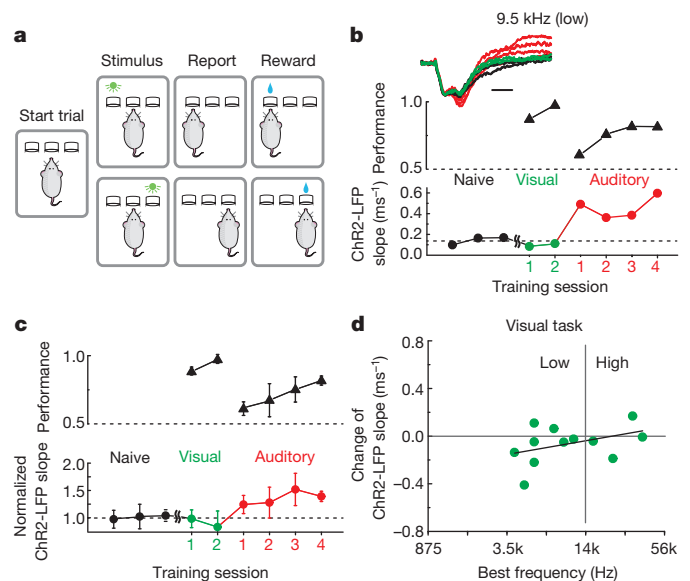


Figure 3 | Potentiation of ChR2-LFP slope is modality specific. **a**, Visual two-alternative forced-choice task. **b**, ChR2-LFP from an example auditory striatum site during visual and auditory task learning, analysed as in Fig. 2a. Scale bar, 2 ms. **c**, Population average of normalized ChR2-LFP slope during visual and auditory task training. **d**, Visual training fails to potentiate auditory striatal input (12 recording sites from four rats; least squares regression, $P = 0.192$).

change -17%; $n = 12$, $P = 0.13$, signed-rank test), and there was no correlation between potentiation and the preferred frequency at the recording site ($n = 12$, $P = 0.19$; Fig. 3d). However, corticostriatal inputs at these same recording sites were potentiated when the animals subsequently learned the auditory cloud-of-tones task (mean potentiation 36%; $n = 6$, $P = 0.03$, signed-rank test; Fig. 3b, c). We therefore conclude that the selective potentiation of auditory corticostriatal synaptic strength is specific to the acquisition of the auditory task.

The preferential potentiation *in vivo* of striatal sites tuned to low frequencies suggested that the pattern of potentiation might be spatially organized within the striatum. We therefore developed an *in vitro* brain slice preparation to examine this possibility. We first characterized the tonotopic organization of the auditory corticostriatal projection by injecting adeno-associated viruses encoding either red or green fluorescent proteins at two different positions along the auditory cortical tonotopic axis. Cortical axons terminated in the striatum in distinct bands, with cortical projections tuned to high frequency sounds terminating more laterally in the auditory striatum and projections tuned to low-frequency sounds more medially (Fig. 4a and Extended Data Fig. 5). We next developed a protocol to assess the gradient of corticostriatal potentiation along the tonotopic axis, by recording ChR2-LFPs in coronal slices that preserve striatal tonotopy (Fig. 4b, see Methods). These recordings targeted left striatum, contralateral to the reward direction associated with low-frequency stimuli (LowRight; $n = 7$ rats). For consistency across experiments, we used only a single slice from each animal, selected on the basis of striatal and hippocampal landmarks (see Methods). ChR2-LFPs in these slices showed a stereotyped waveform similar to that observed *in vivo*, and pharmacological dissection confirmed that the late component of the response was mediated mainly by AMPA (α -amino-3-hydroxy-5-methyl-4-isoxazole propionic acid)-type glutamate receptors (Fig. 4c). Simultaneous extracellular and intracellular recording indicated that the ChR2-LFP was a faithful measure of synaptic strength (Fig. 4d, e, top). As expected, the normalization corrected for changes in ChR2-LFP induced by recruiting more presynaptic fibres (Fig. 4e, bottom), but did not obscure true changes in synaptic strength induced by changes in release probability (Fig. 4d, bottom).

To measure gradients in synaptic strength along the tonotopic axis induced by training, in each slice we recorded the ChR2-LFP at between

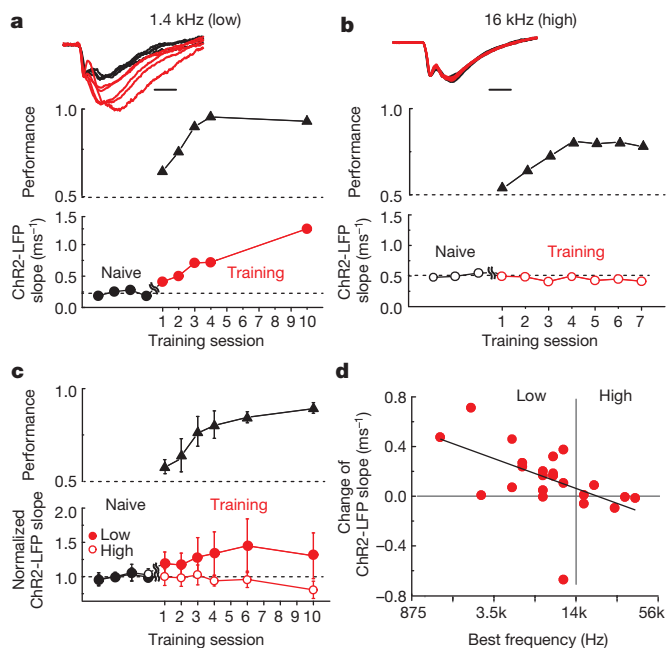


Figure 2 | Frequency-selective potentiation of corticostriatal ChR2-LFP slope during learning. **a, b**, ChR2-LFP (LFP slope: see Methods) before (black) and during (red) training at example sites tuned to low (**a**) and high frequency (**b**). Session 1 is defined as the first session in which the animal performed the full task (see Methods). Scale bars, 2 ms. **c**, Population average of normalized (see Methods) ChR2-LFP slope during learning for sites tuned to low (<14 kHz, $n = 16$ sites, filled circles) and high (>14 kHz, $n = 6$ sites, open circles) frequencies. Mean \pm s.e.m. **d**, Potentiation is restricted to sites tuned to low (<14 kHz) frequencies (23 recording sites from eight rats; least squares regression of potentiation against frequency, $P = 0.011$).

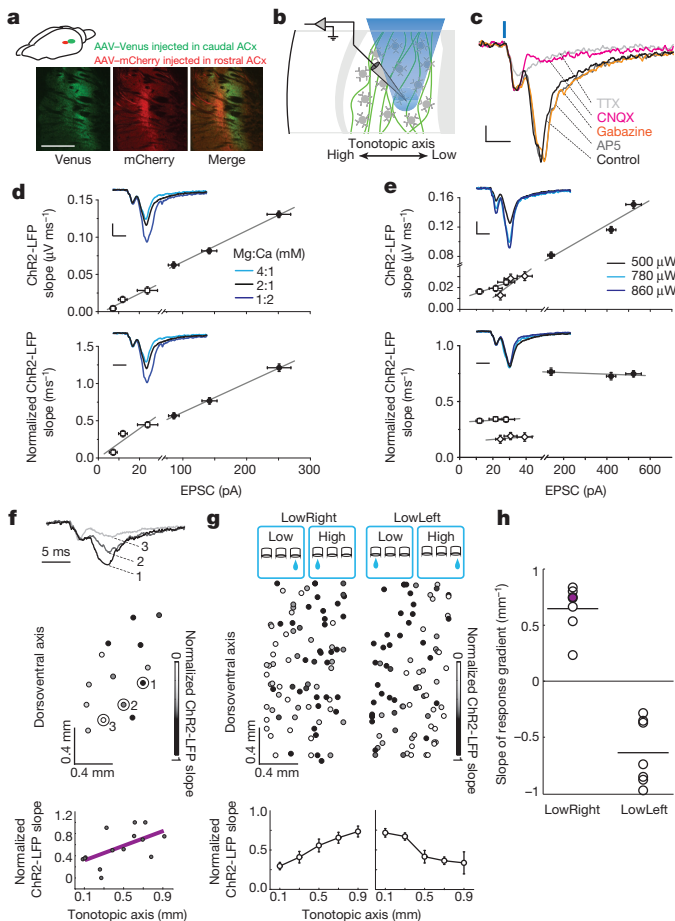


Figure 4 | Gradient of corticostriatal ChR2-LFP slopes encodes the association between stimulus and action. **a**, Tonotopy of projections from auditory cortex to striatum. Scale bar, 1 mm. **b**, Recording method. Light spot (blue) activates a subset of ChR2-expressing corticostriatal axons (green) near recording site. **c**, Pharmacological dissection of ChR2-LFP in a striatal slice. Scale bars, 50 μ V and 5 ms. **d**, Paired *in vitro* excitatory postsynaptic current and LFP at different external divalent ion concentrations. Slopes of LFP measured from raw traces (upper row) and normalized traces (lower row) changed linearly with excitatory postsynaptic current amplitudes ($R^2 = 0.96$ and 0.99 for circles, $R^2 = 0.94$ and 0.81 for squares in upper and lower row respectively; grey lines in right panels are linear regression fits for each recording pair). **e**, Paired recording at different light levels. Slopes of the LFPs measured from raw traces (upper row) changed monotonically with excitatory postsynaptic current amplitudes ($R^2 = 0.94$ for filled circles, $R^2 = 0.91$ for squares and 0.77 for diamonds). Slopes of the normalized LFPs remain constant (lower row). Scale bars for **d** and **e**, 100 μ V and 5 ms. **f**, Normalized ChR2-LFP recorded at many sites within a striatal slice. Sample waveforms (1–3) shown above. ChR2-LFP slope increases with position along tonotopic axis (lower panel). **g**, Population data for LowRight ($n = 7$ rats) and LowLeft ($n = 7$ rats). Error bars, s.e.m. **h**, Gradient correctly identifies learned association in 14 out of 14 individual rats (binomial test $P = 0.00006$). Slope of example shown in **f** is indicated in purple. Bars, mean values.

8 and 16 sites (12.1 ± 2.1). Naive rats showed no systematic difference in the strength of cortical input along the striatal tonotopic axis (Extended Data Fig. 6). In contrast, in rats trained to associate low frequencies with rightward choices, the evoked corticostriatal response was strongest at medial (low frequency) sites and decreased laterally (Fig. 4f, g). This confirmed our observations *in vivo* and was consistent with the association to contralateral rewards. Thus, the degree of corticostriatal synaptic potentiation induced by learning depended systematically on the position along the striatal tonotopic axis.

If the gradient of potentiation along the striatal tonotopic axis encodes the association between frequency and choice direction, then animals

trained to make the opposite association should have a gradient of opposite sign. To test this we trained a new cohort of animals to associate low frequencies with leftward choices (LowLeft; $n = 7$ rats). As predicted, the gradient in these animals was of similar magnitude but opposite in sign (Fig. 4g). There was no difference between these two training groups in ChR2-LFP across the orthogonal (dorsoventral) axis ($P = 0.22$, paired t -test; Extended Data Fig. 7). Thus the spatial gradient of corticostriatal potentiation induced by learning along the tonotopic axis depends on the training contingencies to which the animal is subjected.

Finally, we wondered whether the direction of the stimulus–response association could be inferred on the basis of the sign of the ChR2-LFP gradient in individual animals. Remarkably, the training history (LowRight versus LowLeft) of every rat (14 out of 14) could be correctly inferred from the sign of gradient in a single slice (binomial test $P = 0.00006$, Fig. 4h). The correlation between synaptic strength and tonotopic position reached statistical significance ($P < 0.05$) in 6 out of 14 slices. Thus post-mortem study of corticostriatal efficacy can reliably reveal the training history of individual subjects.

Our results suggest a simple model of how the specific pattern of corticostriatal potentiation we observed might mediate task acquisition. In the LowRight task, training selectively potentiated corticostriatal synapses tuned to low frequencies between the left auditory cortex and the left auditory striatum (Extended Data Fig. 8). Thus in behaving animals, low-frequency tones would trigger stronger activation in the left auditory striatum and direct the animal to the right (contralateral) response port, possibly through the action of direct pathway medium spiny neurons¹⁰ that project ipsilaterally to the left substantia nigra pars reticulata and in turn to the superior colliculus¹⁶. On the other hand, in LowLeft-trained animals, potentiation would cause the same stimulus to trigger stronger activation in right auditory striatum and direct the animal to the left response port. Although this model ignores much of the complexity of striatal circuitry, it offers a simple framework for understanding our results.

Previous work has demonstrated synaptic^{17–20} or receptive field^{21–26} changes induced by learning. Our results identify a locus of synaptic plasticity during the acquisition of a sensory discrimination task. We focused on auditory frequency discrimination, which allowed us to exploit the spatial organization of auditory corticostriatal connections to relate the tuning of cortical neurons to plasticity. Training selectively enhanced the strength of cortical inputs to establish an orderly gradient of corticostriatal synaptic strength across the striatal tonotopic axis.

The strengthening of a subset of connections, selected from a rich sensory representation, is reminiscent of several powerful models of learning^{27–29}. In these models, even difficult nonlinear classification can be achieved by combining a high-dimensional representation of the stimulus—such as is found in the auditory cortex³⁰—through simple reinforcement learning rules. We speculate that selective strengthening of appropriate corticostriatal synapses would allow animals to categorize a wide range of sensory stimuli—even those that are not mapped topographically in the striatum—and may reflect a general mechanism through which sensory representations guide the selection of motor responses.

Online Content Methods, along with any additional Extended Data display items and Source Data, are available in the online version of the paper; references unique to these sections appear only in the online paper.

Received 22 September 2014; accepted 9 January 2015.

Published online 2 March 2015.

- Znamenskiy, P. & Zador, A. M. Corticostriatal neurons in auditory cortex drive decisions during auditory discrimination. *Nature* **497**, 482–485 (2013).
- Salzman, C. D., Britten, K. H. & Newsome, W. T. Cortical microstimulation influences perceptual judgements of motion direction. *Nature* **346**, 174–177 (1990).
- Roitman, J. D. & Shadlen, M. N. Response of neurons in the lateral intraparietal area during a combined visual discrimination reaction time task. *J. Neurosci.* **22**, 9475–9489 (2002).
- Uchida, N. & Mainen, Z. F. Speed and accuracy of olfactory discrimination in the rat. *Nature Neurosci.* **6**, 1224–1229 (2003).

5. Felsen, G. & Mainen, Z. F. Neural substrates of sensory-guided locomotor decisions in the rat superior colliculus. *Neuron* **60**, 137–148 (2008).
6. Erlich, J. C., Bialek, M. & Brody, C. D. A cortical substrate for memory-guided orienting in the rat. *Neuron* **72**, 330–343 (2011).
7. Raposo, D., Sheppard, J. P., Schrater, P. R. & Churchland, A. K. Multisensory decision-making in rats and humans. *J. Neurosci.* **32**, 3726–3735 (2012).
8. Brunton, B. W., Botvinick, M. M. & Brody, C. D. Rats and humans can optimally accumulate evidence for decision-making. *Science* **340**, 95–98 (2013).
9. Thompson, J. A. & Felsen, G. Activity in mouse pedunculo-pontine tegmental nucleus reflects action and outcome in a decision-making task. *J. Neurophysiol.* **110**, 2817–2829 (2013).
10. Tai, L. H., Lee, A. M., Benavidez, N., Bonci, A. & Wilbrecht, L. Transient stimulation of distinct subpopulations of striatal neurons mimics changes in action value. *Nature Neurosci.* **15**, 1281–1289 (2012).
11. Barnes, T. D., Kubota, Y., Hu, D., Jin, D. Z. & Graybiel, A. M. Activity of striatal neurons reflects dynamic encoding and recoding of procedural memories. *Nature* **437**, 1158–1161 (2005).
12. Schultz, W. & Dickinson, A. Neuronal coding of prediction errors. *Annu. Rev. Neurosci.* **23**, 473–500 (2000).
13. Reynolds, J. N., Hyland, B. I. & Wickens, J. R. A cellular mechanism of reward-related learning. *Nature* **413**, 67–70 (2001).
14. Yin, H. H. *et al.* Dynamic reorganization of striatal circuits during the acquisition and consolidation of a skill. *Nature Neurosci.* **12**, 333–341 (2009).
15. Malenka, R. C. & Kocsis, J. D. Presynaptic actions of carbachol and adenosine on corticostriatal synaptic transmission studied *in vitro*. *J. Neurosci.* **8**, 3750–3756 (1988).
16. Hikosaka, O., Takikawa, Y. & Kawagoe, R. Role of the basal ganglia in the control of purposive saccadic eye movements. *Physiol. Rev.* **80**, 953–978 (2000).
17. Carew, T. J., Walters, E. T. & Kandel, E. R. Associative learning in *Aplysia*: cellular correlates supporting a conditioned fear hypothesis. *Science* **211**, 501–504 (1981).
18. Rioult-Pedotti, M. S., Friedman, D. & Donoghue, J. P. Learning-induced LTP in neocortex. *Science* **290**, 533–536 (2000).
19. Rumpel, S., LeDoux, J., Zador, A. & Malinow, R. Postsynaptic receptor trafficking underlying a form of associative learning. *Science* **308**, 83–88 (2005).
20. Whitlock, J. R., Heynen, A. J., Shuler, M. G. & Bear, M. F. Learning induces long-term potentiation in the hippocampus. *Science* **313**, 1093–1097 (2006).
21. Finnerty, G. T., Roberts, L. S. & Connors, B. W. Sensory experience modifies the short-term dynamics of neocortical synapses. *Nature* **400**, 367–371 (1999).
22. Trachtenberg, J. T. *et al.* Long-term *in vivo* imaging of experience-dependent synaptic plasticity in adult cortex. *Nature* **420**, 788–794 (2002).
23. Froemke, R. C., Merzenich, M. M. & Schreiner, C. E. A synaptic memory trace for cortical receptive field plasticity. *Nature* **450**, 425–429 (2007).
24. Hofer, S. B., Mrsic-Flogel, T. D., Bonhoeffer, T. & Hubener, M. Experience leaves a lasting structural trace in cortical circuits. *Nature* **457**, 313–317 (2009).
25. Fritz, J., Shamma, S., Elhilali, M. & Klein, D. Rapid task-related plasticity of spectrotemporal receptive fields in primary auditory cortex. *Nature Neurosci.* **6**, 1216–1223 (2003).
26. Edeline, J. M. & Weinberger, N. M. Receptive field plasticity in the auditory cortex during frequency discrimination training: selective retuning independent of task difficulty. *Behav. Neurosci.* **107**, 82–103 (1993).
27. Maass, W., Natschlag, T. & Markram, H. Real-time computing without stable states: a new framework for neural computation based on perturbations. *Neural Comput.* **14**, 2531–2560 (2002).
28. Sussillo, D. & Abbott, L. F. Generating coherent patterns of activity from chaotic neural networks. *Neuron* **63**, 544–557 (2009).
29. Cortes, C. & Vapnik, V. Support-vector networks. *Mach. Learn.* **20**, 273–297 (1995).
30. Hromádka, T., Deweese, M. R. & Zador, A. M. Sparse representation of sounds in the unanesthetized auditory cortex. *PLoS Biol.* **6**, e16 (2008).

Acknowledgements We thank B. Burbach for technical help, R. Eifert for mechanical material support, and J. Cohen for training the rats. AAV-CAGGS-ChR2-Venus was provided by K. Svoboda. We thank U. Livneh and A. Reid for discussions. This work was supported by grants (R01DC012565 and R01NS088649) from the National Institutes of Health and the Swartz Foundation (A.M.Z.).

Author Contributions Q.X., P.Z., and A.M.Z. designed the experiments; Q.X. performed the experiments; Q.X., P.Z., and A.M.Z. analysed the data and wrote the manuscript.

Author Information Reprints and permissions information is available at www.nature.com/reprints. The authors declare no competing financial interests. Readers are welcome to comment on the online version of the paper. Correspondence and requests for materials should be addressed to A.M.Z. (zador@cshl.edu).

METHODS

No statistical methods were used to predetermine sample size.

Animals and viruses. Animal procedures were approved by the Cold Spring Harbour Laboratory Animal Care and Use Committee and performed in accordance with National Institutes of Health standards. AAV-CAGGS-ChR2-Venus serotype 2/9 was packaged by the University of Pennsylvania Vector Core.

Long Evans male rats (Taconic Farm) were anaesthetized with a mixture of ketamine (50 mg per kg) and medetomidine (0.2 mg per kg), and injected with virus at 3–4 weeks old in the left auditory cortex. To cover most of the area and layers of the primary auditory cortex, three or four injections were made perpendicularly to the brain surface at 1, 2, and 3 mm caudal to the temporoparietal suture, and 1 mm from the ventral edge. Each injection was made at three depths (500, 750, and 1,000 μm), expelling approximately 200 nl of virus at each depth.

Behavioural training. Rats were placed on a water deprivation schedule and trained to perform an auditory two-alternative forced-choice task in a single-walled sound-attenuating training chamber as described previously¹. Briefly, freely moving rats were trained to initiate a trial by poking into the centre port of a three-port operant chamber, which triggered the presentation of a stimulus. Subjects then selected the left or right goal port. Correct responses were rewarded with water. The cloud-of-tones stimulus consisted of a stream of 30-ms overlapping pure tones presented at 100 Hz. The stream of tones continued until the rat withdrew from the centre port. Eighteen possible tone frequencies were logarithmically spaced from 5 to 40 kHz. For each trial either the low stimulus (5–10 kHz) or high stimulus (20–40 kHz) was selected as the target stimulus, and the rats were trained to report low or high by choosing the correct side of port for water reward. In the LowLeft task, the rats were required to go to the left goal port for water reward when the low stimulus was presented, and to the right goal port when high stimulus was presented. In the LowRight task, the rats were required to go to the right goal port when the low stimulus was presented, and to the left goal port when the high stimulus was presented.

The pre-stimulus delay was drawn from exponential distribution with a mean of 300 ms. Early withdrawal from the centre port before the onset of stimuli terminated the trial and a new trial was started. To complete a trial after exiting the centre port, the animals were allowed up to 3 s to select a reward port. Typically, they made their choice within 300–700 ms. Error trials, where the rats reported to the wrong goal port after the presentation of the stimulus, were penalized with a 4 s time-out.

The intensity of individual tones was constant during each trial. To discourage rats from using loudness differences in discrimination, tone intensity was randomly selected on each trial from a uniform distribution between 45 and 75 dB (sound pressure level) during training.

Implanted rats were water deprived and given free water for 1 h every day before ChR2-LFP recording. These sessions were used to record baseline ChR2-LFP responses and defined as naive sessions. Once a stable baseline was achieved, we began training subjects to perform the cloud-of-tones task. To introduce the subjects to the task structure, they were first trained ('direct mode') to poke at the centre port, which triggered the presentation of a stimulus and elicited water delivery from the corresponding goal port. Direct mode training was continued until a subject completed at least 150 trials in a single session (usually the first or second session). In subsequent sessions, defined as 'session 1' in Figs 2 and 3, the animal was trained on the 'full task', in which water was delivered only if the subject poked the correct goal port. For control subjects used in Fig. 3, animals were trained in the direct mode with visual stimuli before introducing the full visual task, and then trained on the full auditory task.

Tetrode recording and optogenetics. Custom tetrode and optic fibre arrays were assembled as described previously¹. Each array carried six individually movable microdrives. Each microdrive consisted of one tetrode (4 polyimide-coated nichrome; wire diameter 12.7 μm ; Kanthal Palm Coast) twisted together and gold-plated to an impedance of 0.3–0.5 M Ω at 1 kHz) and one optic fibre (62.5 μm diameter with a 50- μm core; Polymicro Technologies). The tetrode and fibre on the same microdrive were glued together, with the tips approximately 100 μm from each other.

To implant the tetrode/fibre array, rats were anaesthetized with a mixture of ketamine (50 mg per kg) and medetomidine (0.2 mg per kg) and placed in a stereotaxic apparatus. A craniotomy was made above the target area (2.5–3.5 mm from the bregma and 4–6 mm lateral from the midline). All rats were implanted in left hemisphere. The array was fixed in place with dental acrylic, and the tetrodes were lowered down to auditory striatum (3–5 mm from pia).

Electrical signals in the auditory striatum were recorded using a Neuralynx Cheetah 32-channel system and Cheetah data acquisition software. For action potential recording, signals were filtered 600–6,000 Hz. For LFP recording, signals were filtered 10–9,000 Hz. The rise time of the ChR2-LFP is relatively fast, so to preserve its dynamics we sought to stay as close to the raw data as possible. We re-analysed the data in Fig. 2a using two other choices of offline filter (median, 660-ms window and Butterworth lowpass 1–800 Hz). As shown in Extended Data Fig. 9a, b, although filtering

does affect the details of the ChR2-LFP shape (especially the earliest component), the results are qualitatively unchanged (Extended Data Fig. 9c).

To determine the preferred sound frequency of recording sites, pure tones spanning 1–64 kHz were presented to rats before the start of behavioural training in a soundproof chamber for 100 ms every 2 s, in a random order at 30, 50 or 70 dB (sound pressure level)¹. The multi-unit baseline-subtracted firing rate in a window 5–55 ms after sound onset was compared with that in a window 0–50 ms before sound onset; only sites that significantly responded to sound were included. Firing rates in the window 5–55 ms after sound onset were computed for each frequency at 70 dB, and the peak of the resulting tuning curve was selected as the preferred frequency.

For ChR2-LFP recording, 473 nm laser light was delivered through an FC/PC patch cord using a FibrePort Collimator (Thor Labs) to each implanted fibre individually. ChR2-LFP was recorded immediately after each training session. The laser power out of the patch cord was measured and adjusted to elicit an LFP with clear early and delayed components at each recording site (1–10 mW). For individual recording sites, laser power was adjusted slightly between days to maintain the early, presynaptic component of the LFP response at a consistent level. Each light pulse was 100 μs in duration, presented at 1 Hz, and each recording was an average of approximately 100 trials.

In vivo pharmacology. To dissect the components of ChR2-LFP *in vivo*, rats were anaesthetized and placed in a stereotaxic apparatus. A single tetrode/fibre bundle was placed on a motorized manipulator (Sutter Instrument Company) and the tips of tetrode/fibre were guided to the auditory striatum. Glass pipettes were used to deliver chemicals into the auditory striatum. The pipettes filled with the desired chemicals were carefully moved to penetrate through the cortex and were placed with the tips close to the auditory striatum. Air pressure was slowly applied to inject the chemicals into tissue through a syringe that was connected to the pipette.

Slice recording. Virus-injected and trained rats were anaesthetized and decapitated, and the brains were transferred to a chilled cutting solution composed of (in mM) 110 choline chloride, 25 NaHCO₃, 25 D-glucose, 11.6 sodium ascorbate, 7 MgCl₂, 3.1 sodium pyruvate, 2.5 KCl, 1.25 NaH₂PO₄, and 0.5 CaCl₂. Coronal slices (350 μm) were cut and transferred to artificial cerebrospinal fluid containing (in mM) 127 NaCl, 25 NaHCO₃, 25 D-glucose, 2.5 KCl, 4 MgCl₂, 1 CaCl₂, and 1.25 NaH₂PO₄, aerated with 95% O₂ 5% CO₂.

To ensure maximal alignment across animals, only a single slice (350 μm thickness, between 2.5 and 2.9 mm from the Bregma) per animal was used. Slices were incubated at 34 °C for 15–20 min and then kept at room temperature (22 °C) during the experiments. LFPs were recorded using Axopatch 200B amplifiers (Axons Instruments, Molecular Devices).

We delivered light pulses through a light guide microscope illumination system (Lumen Dynamics) modified to accept a blue laser (473 nm, Lasermate Group) in place of the lamp. The laser beam was focused onto the sample through the $\times 60$ objective during recordings, with an illumination field of 350 μm diameter. Each light pulse was 500 μs at 1 Hz, and each recording was an average of approximately ten trials. Laser power was adjusted from site to site to maintain a similar level of axonal stimulation as judged by the amplitude of the early, presynaptic component of the ChR2-LFP response. To minimize the contribution of rundown on the estimation of the plasticity gradient within the striatal slice, recording locations were selected randomly for each slice.

For drug application, 50 μM AP5, 5 μM Gabazine, 50 μM CNQX, and 0.5 μM TTX were sequentially delivered through a perfusion system.

Data analysis. All data were analysed in MATLAB.

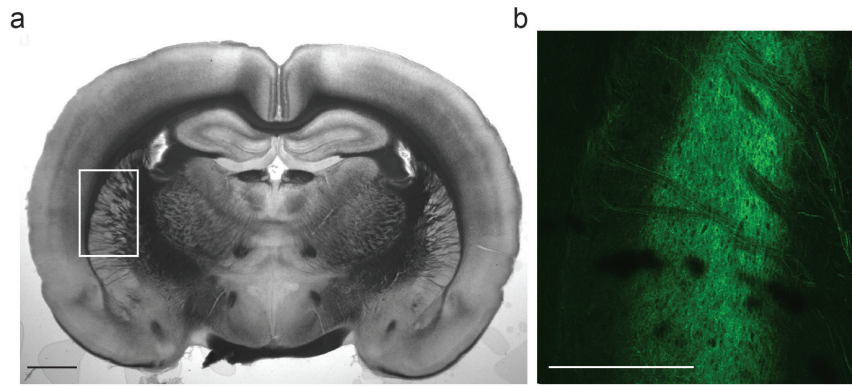
Behaviour analysis only included completed trials. The percentage of correct trials for each animal in each session was computed using the last 200 trials of that session, unless the number of trials was fewer than 300, in which case only the last 100 trials were used.

Each measurement of *in vivo* ChR2-LFP was from a trace obtained by averaging across 70–100 trials (the slope measured from the averaged trace was not different from the averaged slope of single traces; Extended Data Fig. 10). Each average trace was normalized to the peak of the first component (around the time window between 0.5 and 1.2 ms after light stimulation; Extended Data Fig. 2a), and the LFP slope was estimated by a linear regression fit of the rising phase of the second component (Extended Data Fig. 2b; the same time window was used for each recording site across sessions, the time window from site to site varied and was adjusted by eye for each site, ranging from 1.6 to 5 ms after light stimulation). The ChR2-LFP slope for each recording site across sessions was used as a measure of synaptic strength in subsequent analyses (Figs 2a, b and 3b). The absolute change of the ChR2-LFP slope was used in Figs 2d and 3d. In population analyses, normalized synaptic strength for each site was obtained by dividing the LFP slope values from all sessions by the mean of the ChR2-LFP slope values from naive sessions (Figs 2c and 3c).

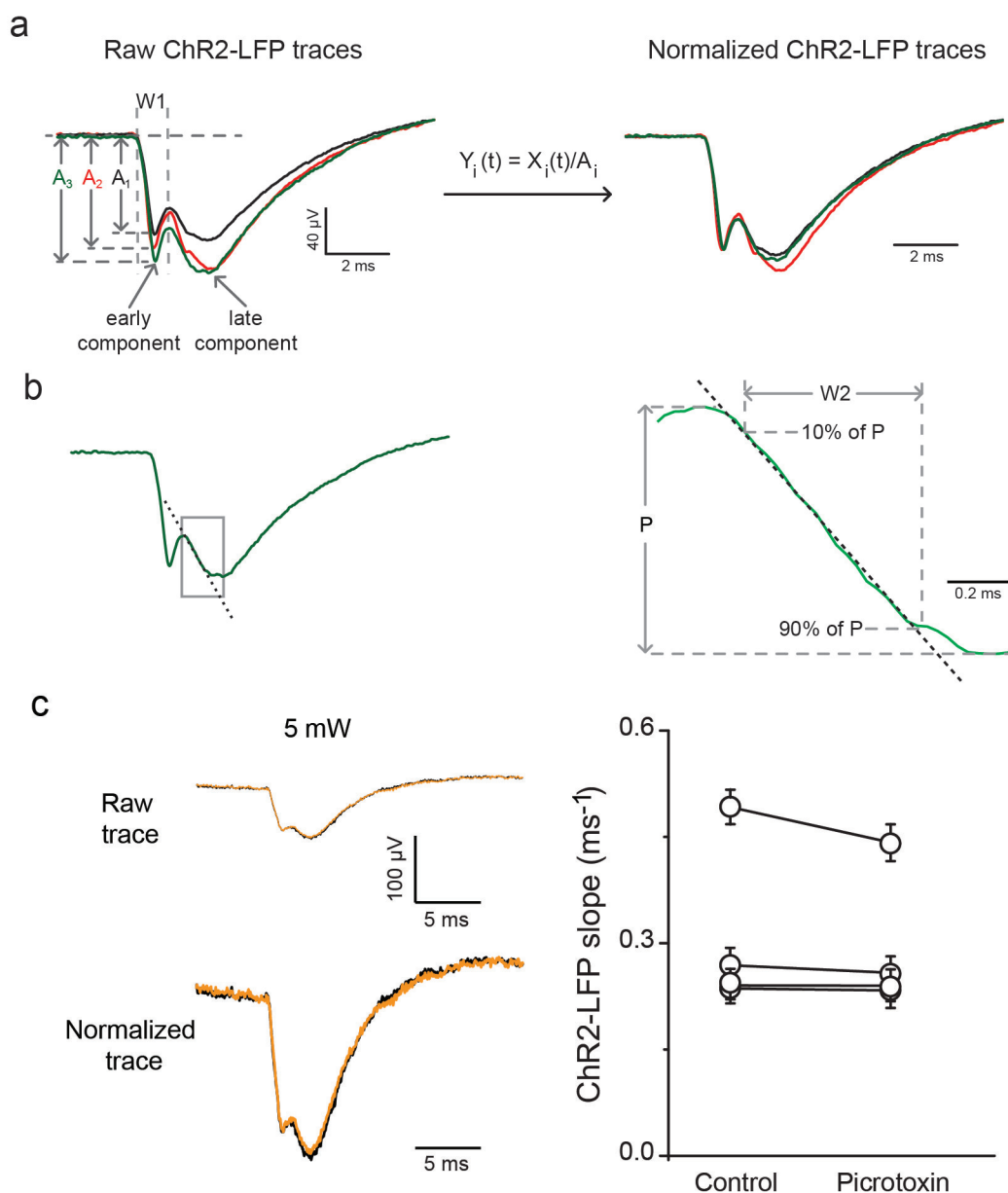
For quantification of the ChR2-LFP in slice recording, the ChR2-LFP slope at each recording site was obtained in a manner similar to that *in vivo*: each averaged trace was normalized to the peak of the first component (around the time window

between 1.5 and 4 ms after light stimulation), and the ChR2-LFP slope was estimated by a linear regression fit of the rising phase of the second component (around the time window between 5 and 8 ms after light stimulation, adjusted by eye for each slice). For each slice, the ChR2-LFP slopes across sites were re-scaled from 0 to 1,

with the smallest ChR2-LFP set to zero and the largest to 1. All recorded brain slices were aligned to a consensus brain slice. The positions of recording sites were measured from the aligned brain slices. Data from all the slices were pooled together for plotting the summary plot and for the quantitative analysis.

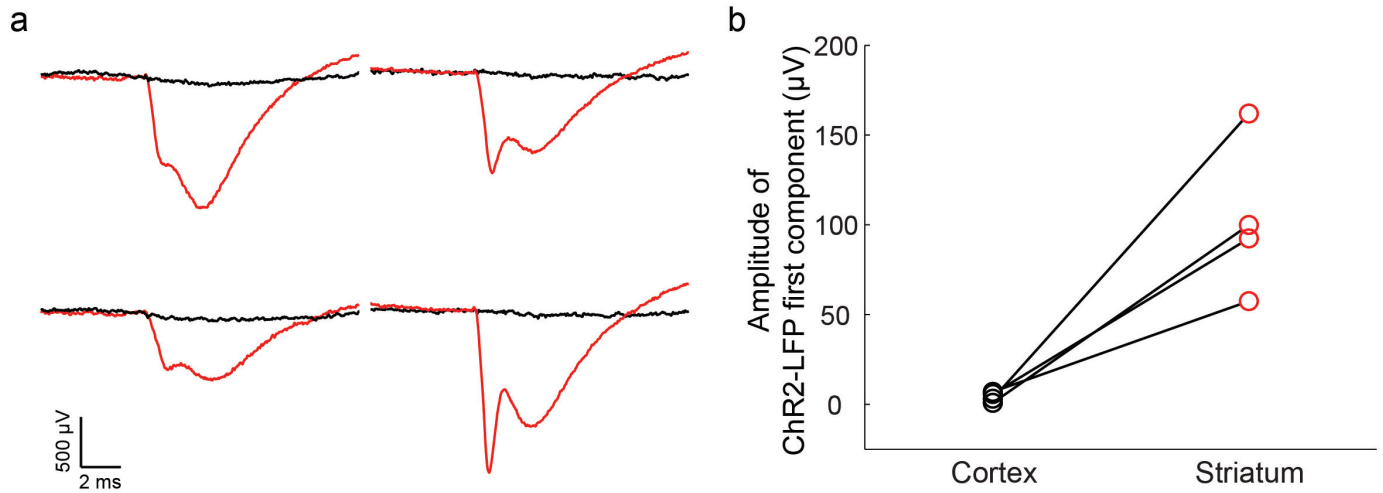


Extended Data Figure 1 | Corticostriatal projections from auditory cortex to striatum. **a**, Coronal view for the location in the striatum that receives auditory cortical inputs. **b**, Confocal image of auditory cortical axon terminals expressing ChR2-Venus in the striatum. Scale bars, 2 mm.



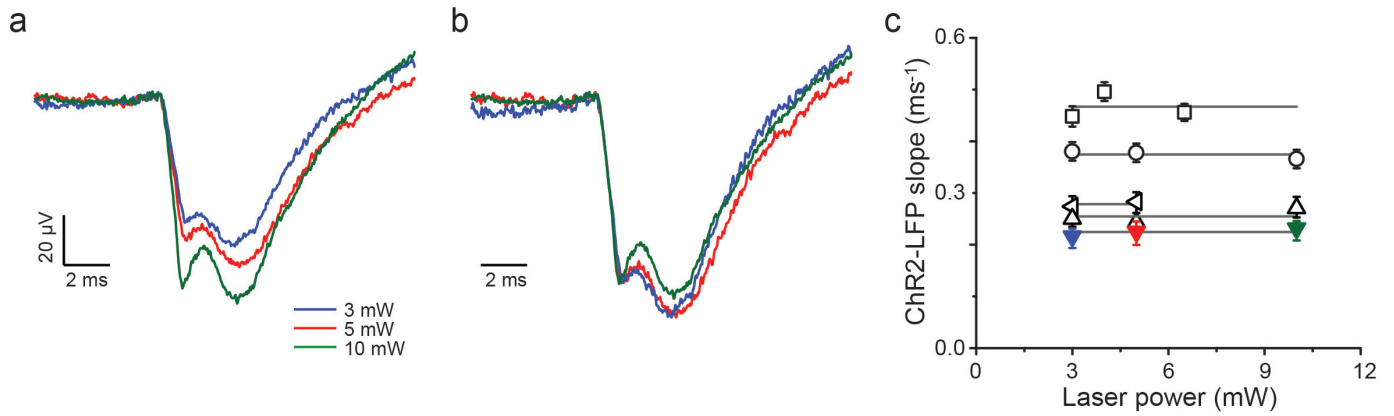
Extended Data Figure 2 | Slope measurement for ChR2-LFP and GABAergic (γ -aminobutyric-acid-mediated) synaptic transmission does not contribute to the ChR2-LFP slope *in vivo*. **a**, Raw ChR2-LFP traces (left) were normalized to the amplitude of their corresponding early component (A_i). The normalization factor A_i was determined as the peak of the raw trace in the time window ($W1$) between 0.5 and 1.2 ms after light stimulation onset. **b**, The rising phase of the late component of ChR2-LFP (in a time window $W2$ defined by rise from 10% to 90% of the peak P) was fitted linearly, and the slope

of the fit was used for the quantification of ChR2-LFP. **c**, Left: ChR2-LFP before (black traces) and after (orange traces) picrotoxin application (20 mM, 5 μ l). Raw traces are averaged traces from 60–80 trials at each condition (upper row). Normalized traces are raw traces normalized to their peaks of first components (as illustrated in **a**). Right: slopes measured from normalized traces in control and picrotoxin conditions for each recording before and after picrotoxin application ($P = 0.8$, paired signed-rank test). Data are presented as mean \pm s.e.m.



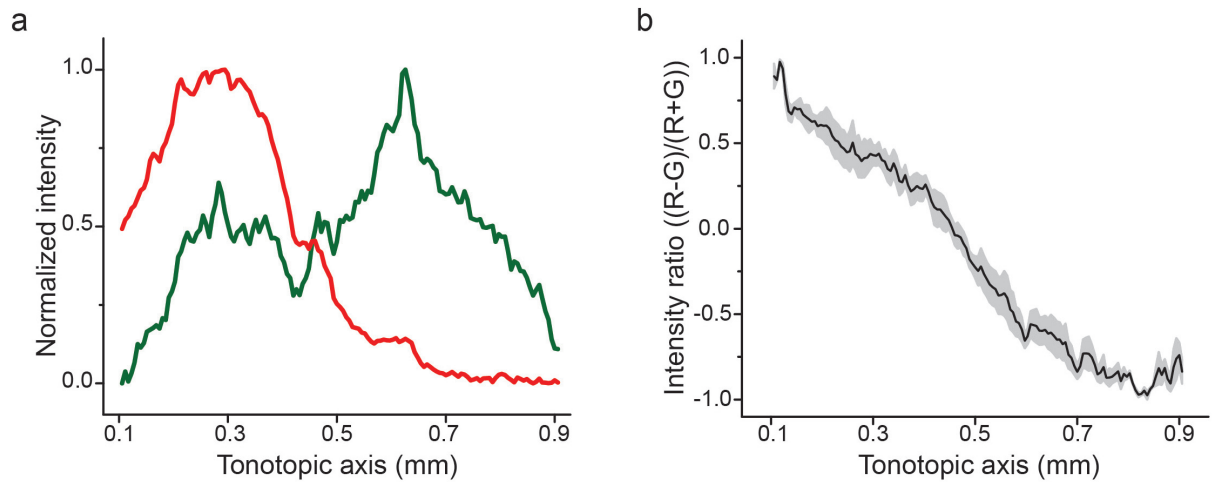
Extended Data Figure 3 | ChR2-LFP depends on the presence of ChR2-expressing axons. To rule out the possibility that the TTX-insensitive component of the light-evoked response resulted from a photoelectric or other artefact, rather than from ChR2-evoked currents, we assessed light-evoked responses in brain regions that did not express ChR2. **a**, Four independent recordings in the auditory striatum (red traces) which receives auditory cortical

input (ChR2-expressing axons are present), and the overlying somatosensory cortex (black traces) which lacks auditory cortical input (ChR2-expressing axons are absent). Each pair of recordings is from the same tetrode/fibre bundle. The recordings indicate that the light artefact was negligible under our conditions. **b**, Comparison of the first component amplitude from each recording pair.

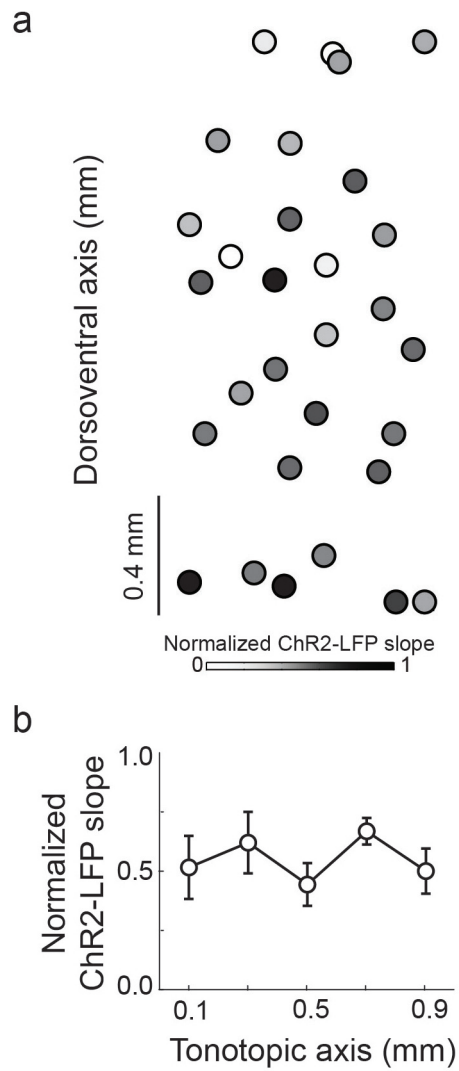


Extended Data Figure 4 | Normalization procedure corrects for variation in light power *in vivo* (for *in vitro* data see Fig. 4d, e). **a**, Example of ChR2-LFP recorded at different light levels. **b**, Normalized ChR2-LFP, the same example as in **a**. **c**, Slopes from five example recordings across 1–10 mW light level range (coloured symbols are examples shown in **a** and **b**). Grey lines are

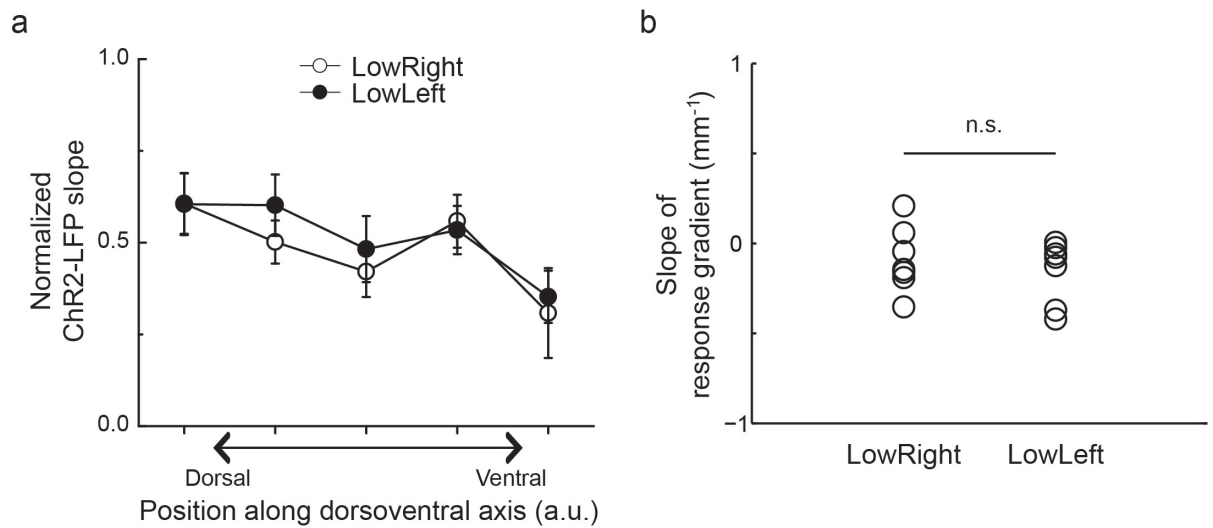
drawn from the mean values of each group. Together with the data shown in Fig. 4e, the normalization procedure thus minimizes fluctuations in the response arising from artefactual changes in the number of recruited fibres, but preserves changes arising from actual increases or decreases in synaptic efficacy.



Extended Data Figure 5 | Quantification of corticostriatal projection topography. a, Normalized red and green fluorescence intensities measured across the tonotopic axis from the image shown in Fig. 4a. b, Mean red:green intensity ratio across the tonotopic axis ($n = 3$ sections from two rats). Shading, s.e.m.

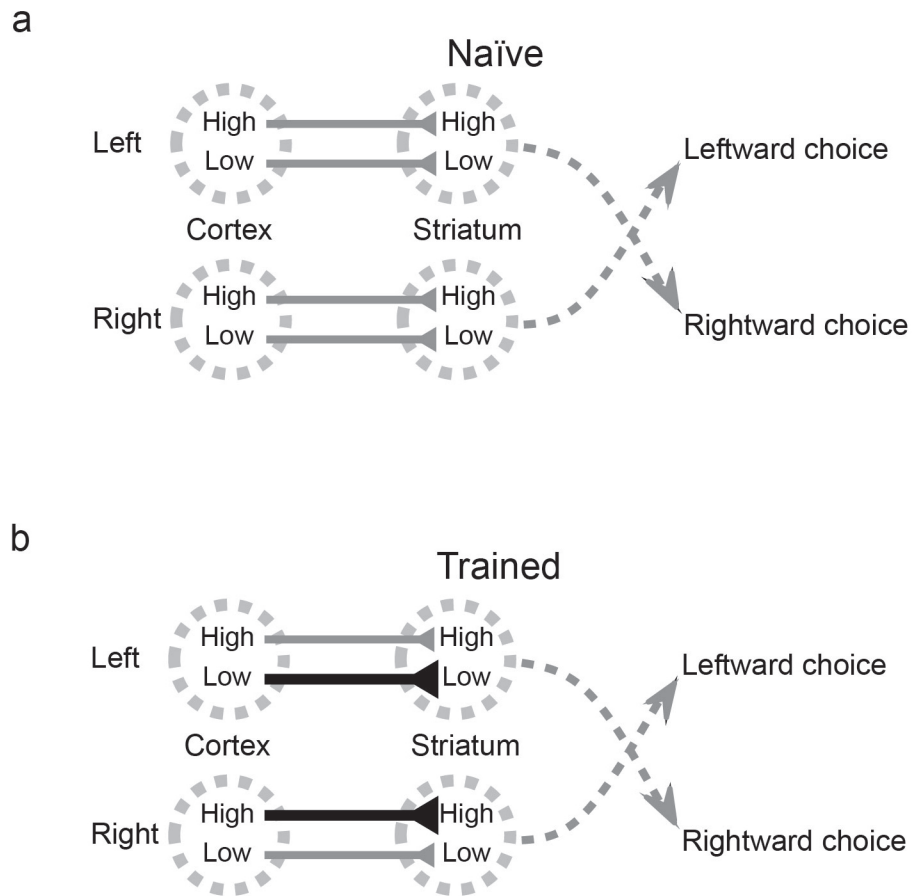


Extended Data Figure 6 | ChR2-LFP slope does not vary systematically across the tonotopic axis in naive rats. **a**, ChR2-LFP slope map from three striatal slices ($n = 3$ rats). **b**, Quantification of the ChR2-LFP slope across the tonotopic axis. Data are mean \pm s.e.m.



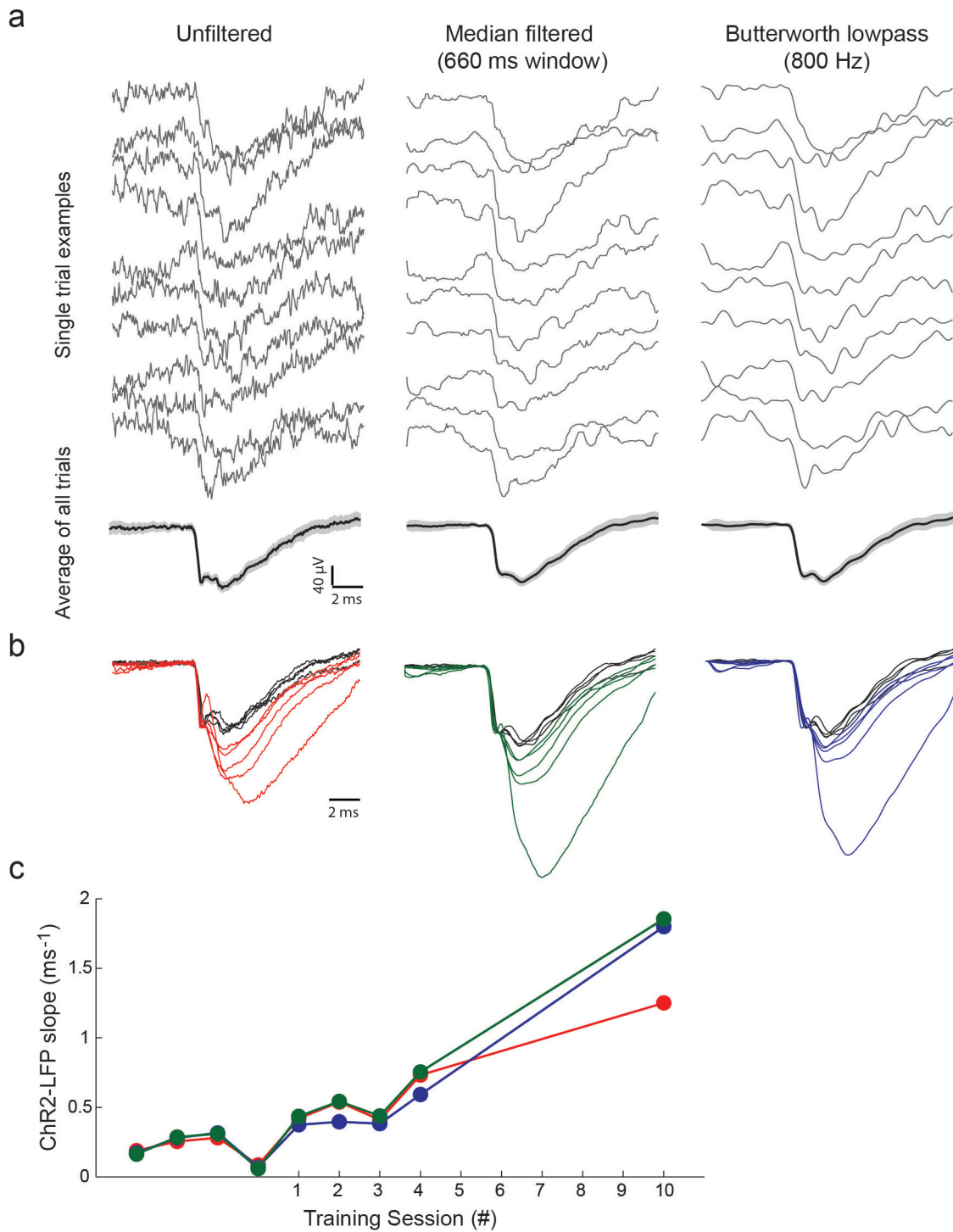
Extended Data Figure 7 | Gradient of ChR2-LFP across the dorsoventral (non-tonotopic) axis showed no difference between the two training groups.
a. Averaged ChR2-LFP slopes with position along the tonotopic axis for

LowRight and LowLeft groups (seven rats from each group). **b.** Individual gradients of ChR2-LFP across the dorsoventral axis from LowRight and LowLeft groups ($P = 0.22$, paired t -test).



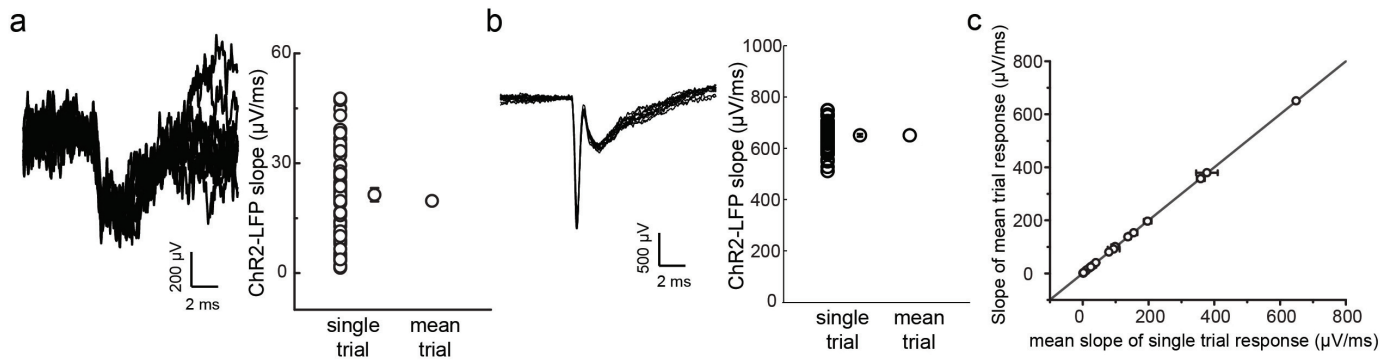
Extended Data Figure 8 | Model showing how corticostriatal potentiation could mediate task acquisition. **a**, In the naive rat, the strength of corticostriatal connections does not depend on their frequency preference. **b**, Training to associate low stimuli with rightward choices and high stimuli

with leftward choices (LowRight) selectively potentiates corticostriatal synapses tuned to low frequencies in the left hemisphere and corticostriatal synapses tuned to high frequencies in the right hemisphere. Thus, in the trained rat, low stimuli drive rightward choices and high stimuli drive leftward choices.



Extended Data Figure 9 | To exclude the possibility that spiking responses affected the Chr2-LFP measurement, we analysed the data after median or lowpass filtering. **a**, Single trial (upper rows) and average (bottom row) examples of unfiltered, median filtered, and Butterworth lowpass filtered

responses. Average traces are presented as mean values (black traces) with 95% confidence intervals (grey shading). **b**, Chr2-LFP examples in Fig. 2a with different filter settings. **c**, Chr2-LFP measurements from examples shown in Fig. 2a at different filter settings.



Extended Data Figure 10 | Changes in ChR2-LFP could result from variation in response timing precision. To rule out this possibility we compared slopes measured from single trial and mean responses. **a**, Single trial responses (left) and slopes measured from individual trials and mean response

(right) at a weakly light-responsive site. **b**, An example robustly responsive site. **c**, Comparison of mean slopes from single trial responses and slopes quantified from mean responses.